Astronomy
&
Astrophysics

Test particle simulation of the Electron Firehose instability

G. Paesold[1,2] and A. O. Benz[1]

[1] Institute of Astronomy, ETH-Zentrum, 8092 Zurich, Switzerland
[2] Paul Scherrer Institute, Würenlingen und Villigen, 5232 Villigen PSI, Switzerland

Abstract. In the course of the energization of electrons to energies of some tens of keV during the impulsive phase of a solar flare, the velocity distribution function of the electrons is predicted to become anisotropic with $T_\parallel^e > T_\perp^e$ (Here, $\parallel$ and $\perp$ denote directions with respect to the background magnetic field). Such a configuration can become unstable to the so-called Electron Firehose instability (EFI). Left hand circularly polarized electromagnetic waves propagating along the magnetic field are excited via a non-resonant mechanism: electrons non-resonantly excite the waves while the protons are in resonance and carry the wave. The non-resonant nature of the instability raises the question of the response of the electron population to the growing waves. Test particle simulations are carried out to investigate the pitch-angle development of electrons injected to single waves and wave spectra. To interpret the simulation results, a drift kinetic approach is developed. The findings in the case of single wave simulations show the scattering to larger pitch-angles in excellent agreement with the theory. The situation dramatically changes when assuming a spectrum of waves. Stochasticity is detected at small initial parallel velocities resulting in significant deviations from drift kinetic theory. It enhances the scattering rate of electrons with initial parallel velocity below to the mean thermal perpendicular velocity. Increased scattering is also noticed for electrons having initial parallel velocity within an order of magnitude of the resonance velocity. The resulting pitch-angle scattering is proposed to be an important ingredient in Fermi-type electron acceleration models, particularly transit-time acceleration by compressional MHD waves.

Key words. acceleration of particules – Sun: flares

1. Introduction

A solar flare is a complex explosive phenomenon in the solar corona. Apparently, magnetic energy is abruptly released, driving bulk mass motion, heating plasma and accelerating electrons and ions to hard X-ray energies and beyond (e.g. Sturrock 1980). Particles are accelerated at many sites throughout the universe but solar flares offer the widest range of observations and allow to probe both, electron and ion acceleration. During solar flares, large amounts of energies ($\sim 10^{28}$ to $\sim 10^{34}$ erg) are released on time scales varying from fractions of seconds to minutes (Kiplinger et al. 1984). The magnitude and energy spectrum in hard X-rays often indicate that much of the released energy goes into the energization of electrons at tens of keV and can extend up to 10 MeV. In addition, observations show that the number of energized electrons are comparable to the electron content of the whole flaring region. The requirement of accelerating such a large number of electrons ($\sim 10^{37}$) within about 10 s (Brown 1971; Moore & Fung 1972) restricts the candidates of accelerators. Currently, possible mechanisms can be roughly divided into three broad classes: *stochastic acceleration by MHD waves, shock acceleration* and *acceleration*

by direct electric fields (dc) (for a review see e.g. Miller et al. 1997).

A common feature of these accelerators is a preference in accelerating particles in the direction parallel to the background magnetic field. Parallel dc electric fields trivially accelerate only along the magnetic field while stochastic scenarios as transit-time damping act via small amplitude magnetic mirroring, which is only capable of transferring energy in parallel direction if no additional scattering mechanism is provided (Lenters & Miller 1998). Works of e.g. Wu (1984) and Leroy & Mangeney (1984) describe the parallel directed energization of electrons at the earths bow shock via shock drift acceleration with quasi perpendicular shocks. The low collision rate in the solar pre-flaring plasma cannot reduce the significant anisotropy in the velocity distribution function of the according particle species (e.g. electrons) that builds up during the acceleration process. When assuming acceleration from a thermal level up to orders of ~ 10 keV, the anisotropy becomes essential.

Some of the acceleration processes mentioned above require pitch-angle scattering in order to operate efficiently, among which is a scenario proposed by Miller et al. (1996) based on transit-time acceleration. The primary energy input is mass motion in form of an outflow with velocities of order of the Alfvén speed resulting from magnetic reconnection events.

Due to its Alfvénic speeds, the outflow can excite turbulence and an MHD cascade is initiated. The cascade transfers the energy from the initial large-amplitude and large-scale MHD waves to small scales and small amplitudes where the energy can be dissipated into thermal electrons, by transit-time damping (Fisk 1976; Stix 1992). Transit-time acceleration can be regarded as a low-amplitude realization of the Fermi process with the main difference, that the wave-particle interaction is, instead of non-resonant magnetic mirroring, of rather resonant nature, i.e. $v_{\parallel} \approx \omega/k_{\parallel}$.

It has been shown (Lenters & Miller 1998) that this mechanism is in need of a pitch angle scattering mechanism in order to operate efficiently. The pitch angle scattering time scale has to be comparable to the characteristic wave-particle interaction time which is given by $\approx \pi/k v_{\mathrm{A}}$, where v_{A} is the Alfvén speed. Pitch-angle scattering by Coulomb collisions is therefore not sufficiently rapid to lead to efficient electron acceleration by transit-time damping (Lenters & Miller 1998). Whistler waves (right-hand circularly polarized waves below Ω_{e}) at a low energy level have been proposed as possible scatterers (Miller 1997). These waves would deliver the desired scattering, but it is unclear whether they are present and what the actual source would be. Since the energization of electrons in impulsive solar flares is essential, a successful acceleration scenario must contain inherently all necessary ingredients. In order to obtain a self-contained picture of electron acceleration during solar flares, the pitch-angle scattering mechanism therefore preferably originates within the acceleration scenario. The anisotropy in the electron velocity distribution described in the paragraph above is a source of free energy and therefore may deliver a possible agent to scatter electrons to higher pitch-angle.

It is known from analyses in linearized kinetic theory (Hollweg & Völk 1970; Pilipp & Völk 1971) that an anisotropic plasma ($T_{\parallel} > T_{\perp}$) can become unstable to the so-called Electron Firehose instability (EFI). The EFI is an extension of the well known (MHD-) Firehose instability, originally mentioned and applied to predict isotropy in the particle distributions of the solar wind by Parker (1958). While the classic Firehose instability is of entirely non-resonant nature, the EFI involves resonant protons with the electrons remaining non-resonant. It has been proposed in a former work (Paesold & Benz 1999) that Electron Firehose (EF) waves may be excited in course of the acceleration processes during solar flares. In addition to the parallel propagating EF mode a new branch of the EFI was found at oblique angles. This mode was further investigated by Li & Habbal (2000). Messmer (2002) showed by using PIC simulations that the parallel EFI is capable to scatter the electrons on short time scales in pitch-angle. He uses large anisotropies to achieve a rapid development. This results in resonant wave-electron interaction, and hence, very efficient pitch-angle scattering is obtained.

The work presented herein focuses on the non-resonant phase of the process. Since the source of free energy lies in the anisotropic distribution function, the instability is expected to isotropize the electron population and to remove the anisotropy. Do electrons just loose parallel energy or are they also scattered in pitch-angle? Which non-resonant processes scatter electrons in velocity? Are all electrons affected equally? Even though the

non-resonant scattering is expected to be less effective than a resonant interaction, an understanding of the non-resonant processes leads to important insights into the plasma behavior near the instability threshold. Before reaching large anisotropies, the instability starts eroding it and the plasma eventually resides in a state close to marginal instability. The non-resonant situation at small electron anisotropies, close to the threshold of the EFI, is probably more realistic for solar applications.

Besides the importance of a possible application to solar flare physics, the EFI poses the fundamental problem of a kinetic description for the electron response to a hydromagnetic instability. The problem is analyzed by drift kinetic theory and by applying test particle simulations. The response of the electrons to the EF wave field, obtained from linearized kinetic theory, is investigated in view of the displacement in velocity space, mostly in pitch-angle.

The plan of the paper is as follows: the linearized kinetic analysis of the EFI is presented in Sect. 2. An analytic description of an electron in an EF wave field is presented in Sect. 3, whereas the test particle simulations are described in Sect. 4. The presentation of the results in Sect. 5 is followed by a discussion in Sect. 6 and the work is summarized in the conclusions in Sect. 7.

2. Electron Firehose instability

The extension of the (MHD-) Firehose instability to higher frequencies, the Electron Firehose Instability (EFI), is non-resonantly excited by the electrons, whereas the protons are now in resonance with the waves. The anisotropy in the electron velocity distribution drives the waves while the protons carry the wave. A typical dispersion relation of the EF waves is displayed in Fig. 1. The mode depicted is parallel propagating, purely transverse and left-hand circularly polarized. The dispersion of the EF waves is computed by IDLWhamp (Paesold 2002), an easy to use IDL interface to the WHAMP code originally developed by Rönnmark (1982). The code provides
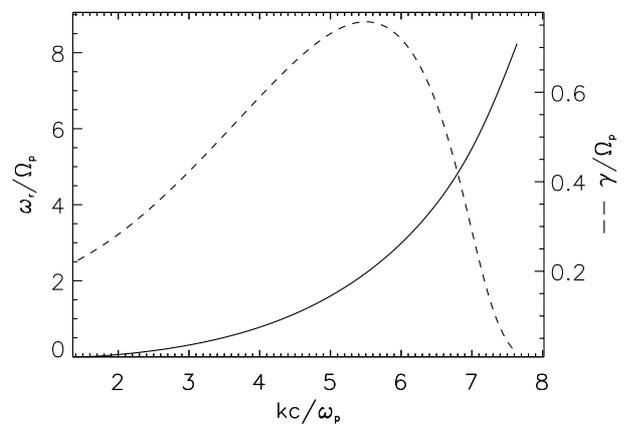
Fig. 1. A typical plot of the dispersion relation of EF waves. The chosen parameters are $T_{\perp}^{\mathrm{e}} = T_{\perp}^{\mathrm{p}} = T_{\parallel}^{\mathrm{p}} = 10^7$ K, $T_{\parallel}^{\mathrm{e}}/T_{\perp}^{\mathrm{e}} = 13, n_{\mathrm{e}} = 5 \times 10^{10}$ cm^{-3}, $B_0 = 100$ G. The real part of the frequency ω_{r} and the growth rate γ are normalized to the proton gyrofrequency $\Omega_{\mathrm{p}} > 0$. The parallel wave vector is normalized to the proton inertial length. The whole branch is fully left-hand circularly polarized.

the user with the full solution of the dispersion equation in linearized kinetic theory. For simplicity, the anisotropy is modeled by maxwellian distributions having $T_\parallel^e > T_\perp^e$, and only the parallel mode is considered.

While the protons have been assumed to remain isotropic in Fig. 1, a proton anisotropy alters the linearized dispersion of the waves. The $k_\parallel$ of maximum growth is shifted towards smaller k with increasing proton anisotropy, and the according frequency ω_r decreases. The mode can also become right-hand circularly polarized at small values of $k_\parallel$ when the proton anisotropy exceeds a threshold value of $T_\parallel^p / T_\perp^p \geq 2$. In the analysis presented herein, a possible proton anisotropy is not taken into account.

3. Analytical theory

The electron displacement in velocity space is determined by the non-resonant interaction with the wave's electromagnetic field, which is decomposed into its parallel component $E_\parallel = \hat{e}_\parallel \cos \Psi$ and two circularly polarized components $E_\pm = \hat{e}_\pm (\cos \Psi, \mp \sin \Psi)$ with amplitudes $\hat{e}_\pm = (E_x \pm E_y)/2$, where $\Psi = k_\parallel z + k_\perp x - \omega t$ is the wave's phase at the location of the electron. The negative subscript refers to left-hand polarized waves. The magnetic field of the wave is obtained via Faraday's law $\dot{\boldsymbol{B}} = -c \boldsymbol{\nabla} \times \boldsymbol{E}$ as $(c/\omega) [\pm(k_\parallel \hat{e}_\pm) \sin \Psi, (k_\parallel \hat{e}_\pm - k_\perp \hat{e}_\parallel) \cos \Psi, \pm(k_\perp \hat{e}_\pm) \sin \Psi]$. The relative phase angle between the electron and the wave is denoted with $\phi_\pm = \theta \pm \Psi$. In the following we assume parallel propagating EF waves and therefore $k_\perp \equiv 0$, $k_\parallel \equiv k$, $\hat{e}_\parallel \equiv 0$ and put $\hat{e}_- \equiv \hat{e}$.

In order to identify the main contributions responsible for the response of the electrons to the waves, adiabaticity is assumed in the analytical approach. Since the wave frequency is much smaller than the cyclotron frequency of the electron, i.e. $\omega_r \approx \Omega_p \ll \Omega_e$, this assumption holds for parallel particle velocities small enough to ensure large frequency separation of the Doppler shifted wave frequency and the electron gyrofrequency. The gyrofrequencies are defined as $\Omega_\alpha = |q_\alpha| B_0 / c m_\alpha$, where α denotes the particle species. In addition, small field strengths have to be assumed for adiabaticity. With these assumptions a *drift kinetic* approach can be chosen (Hasegawa 1975). The according continuity equation in phase space is given by

$$\partial_t f_D + \boldsymbol{\nabla} \cdot (\boldsymbol{v}_D f_D) + \frac{\partial}{\partial v_\parallel} \left(\frac{F_\parallel}{m} f_D \right) = 0, \tag{1}$$

where $f_D(v_\parallel, \mu, \boldsymbol{x}, t)$ is the distribution function of the guiding centers and $\mu = m v_\perp^2 / 2 B_0$ is the magnetic moment. $F_\parallel$ refers to a possible external force in parallel direction to the background magnetic field. This equation is obtained by transforming the Vlasov equations to guiding center coordinates and by time averaging over the fast gyration of the electrons. In the following, when speaking of quasi-particles, we refer to the gyro centers of the electrons. The drift velocity $\boldsymbol{v}_D$ can be split into parallel and perpendicular components and contains several different contributions as e.g. $E \times B$ drift, curvature drift and polarization drift. Whereas the latter drift is negligible for the situation

assumed herein, the relevant drifts are the $E \times B$ and the curvature drift given by

$$\boldsymbol{v}_E = \frac{(c \boldsymbol{E} + \boldsymbol{v}_\parallel \times \boldsymbol{B}) \times \boldsymbol{B}}{B^2}, \tag{2}$$

$$\boldsymbol{v}_C = \frac{m_e c v_\parallel^2}{q B^4} [\boldsymbol{B} \times (\boldsymbol{B} \cdot \boldsymbol{\nabla}) \boldsymbol{B}], \tag{3}$$

where the parallel direction refers to $\boldsymbol{B}_0$. The modification involving the parallel velocity in the $E \times B$ drift has to be taken into account when assuming additional perpendicular magnetic fields (Hasegawa 1975). Assuming $\boldsymbol{E} = \delta \boldsymbol{E}$ and $\boldsymbol{B} = \boldsymbol{B}_0 + \delta \boldsymbol{B}$, where $\delta \boldsymbol{E}$ and $\delta \boldsymbol{B}$ are the wave components, Eqs. (2) and (3) yield, keeping only contributions of first order in the perturbation, a total drift in perpendicular direction

$$\boldsymbol{v}_{D_\perp} = \frac{c \hat{e} B_0}{B^2}$$
$$\times \left[1 - \frac{v_\parallel}{c} \left(\frac{ck}{\omega} \right) - \frac{m_e v_\parallel^2 \omega B_0}{ce B^2} \left(\frac{ck}{\omega} \right)^2 \right] \tag{4}$$
$$\times (\sin \Psi, -\cos \Psi),$$

and accordingly, when taking second order contributions into account, the resulting drift in parallel direction

$$v_{D_\parallel} = \frac{c \hat{e}^2}{B^2} \left(\frac{ck}{\omega} \right)$$
$$\times \left[1 - \frac{v_\parallel}{c} \left(\frac{ck}{\omega} \right) - \frac{m_e v_\parallel^2 \omega B_0}{ce B^2} \left(\frac{ck}{\omega} \right)^2 \right]. \tag{5}$$

Equating the expression in the brackets in Eqs. (4) and (5) to zero, directly yields a critical velocity v_{crit} in parallel and perpendicular direction where the contributions are in balance and result in zero drift. Expanding the numerator of v_{crit} for $(B_0/B)^2 \ll \Omega_e/\omega$ yields as the only physical solution

$$v_{crit} \approx \frac{\omega}{k}, \tag{6}$$

the phase velocity of the wave. The drift in parallel direction below the critical velocity v_{crit} is in positive direction and changes sign above it. The magnitude of the perpendicular drift $v_{D_\perp} = |\boldsymbol{v}_{D_\perp}|$ has a minimum (here equal to zero) at v_{crit}. The explanation is straight forward: since the particle propagates at the same parallel speed as the wave, the resulting $E \times B$ drift contributions cancel. There is no relative velocity between wave and particle, hence the particle experiences no curvature drift as well. Note, that the critical velocity does not depend on the wave field strengths.

The resulting quasi-particle pitch-angle can readily be obtained by computing

$$\alpha_c = \arctan \left(\frac{v_{D_\perp}}{v_\parallel^0 + v_{D_\parallel}} \right). \tag{7}$$

When assuming a wave field of N waves indexed by i with constant amplitudes $\hat{e}_i = \hat{e}$, Eqs. (4) and (5) have to be modified. In analogy to a random walk in the $v_x - v_y$-plane, the resulting rms drift in perpendicular direction is then given by

$$v_{D_\perp} = \sqrt{\sum_{i=1}^N \boldsymbol{v}_{D_\perp, i}^2}, \tag{8}$$

where $\boldsymbol{v}_{D_\perp,i}$ is the drift contribution given by Eq. (4) for each wave i. It has been assumed, that N is a large number and that the time the particle stays in the wave field is long enough to sample the largest wavelength in the spectrum. The average parallel drift is obtained as

$$v_{D_\parallel} = \frac{c\hat{e}^2}{B^2} \sum_{i=1}^{N} \left(\frac{ck_i}{\omega_i}\right)$$
$$\times \left[1 - \frac{v_\parallel}{c}\left(\frac{ck_i}{\omega_i}\right) - \frac{m_e v_\parallel^2 \omega_i B_0}{ceB^2}\left(\frac{ck_i}{\omega_i}\right)^2\right]. \quad (9)$$

The squared magnitude of the total magnetic field $B^2 = |\boldsymbol{B}|^2$ is given by $B^2 = B_0^2 + \sum(\hat{e}ck_i/\omega_i)^2$. The drift velocities in Eq. (7) have to be adapted accordingly to obtain the pitch-angles of the particles in the wave field.

In the case of a wave spectrum, a critical velocity cannot be defined as easily as in the single wave case. An estimate for $v_{\rm crit}$ in case of a wave field can be obtained by determining the minimum in Eq. (8) or the zero of Eq. (9) in dependence on $v_\parallel$.

An important quantity has been omitted in the derivation above. Contrary to the single wave case, the modulus of the total instantaneous magnetic field of the wave spectrum changes as the particle propagates. Since the motion is assumed to be adiabatic, the particle's magnetic moment is an invariant. When changing the modulus of the magnetic field by $\Delta|B|$, the resulting shift in parallel velocity is approximately given by

$$\Delta v_\parallel^\mu \approx -\frac{1}{2}\frac{v_\perp^0}{v_\parallel^0}\frac{\Delta|B|}{|B_0|}v_\perp^0. \quad (10)$$

Here it is assumed that $\Delta v_\perp^0 \ll v_\perp^0$, $\Delta|B| \ll |B_0|$ and that energy is approximately conserved on the average. The first requirement is only true for electrons with non-vanishing initial perpendicular speed. It is not possible to include $v_\parallel^\mu$ in the drift kinetic approximation since $\Delta|B|$ varies individually for each particle and depends on the relative phases of the applied wave fields. Invariance of the magnetic moment causes a random scatter of the particles and can qualitatively explain the deviation of the simulation results presented in Sect. 5.2 from the predictions of Eqs. (7), (8) and (9).

4. Test particle simulation

4.1. Simulation setup

The relativistic equations of motion for a particle of charge q and mass m in a field of N waves and a homogeneous background magnetic field B_0 are given by

$$\frac{d\boldsymbol{p}}{dt} = q\frac{\boldsymbol{v}}{c}\times\boldsymbol{B}_0 + q\sum_{i=1}^{N}\left(\boldsymbol{E}_i + \frac{\boldsymbol{v}}{c}\times\boldsymbol{B}_i\right), \quad (11)$$

$$\frac{d\boldsymbol{x}}{dt} = \boldsymbol{v}, \quad (12)$$

where $\boldsymbol{x}$ is the particle position vector, $\boldsymbol{v}$ the velocity and $\boldsymbol{E}_i$ and $\boldsymbol{B}_i$ are the electric and magnetic fields of the wave i propagating parallel to $\boldsymbol{B}_0$.

Test particle trajectories are calculated by integrating a dimensionless form of Eqs. (11) and (12) with a standard leap-frog mover following Birdsall & Langdon (1991) (at half time step: acceleration with an extrapolated electric field, rotation around the instantaneous magnetic field, including the wave field and acceleration with updated velocities). The code used herein is a leap-frog version of the code used by Miller & Viñas (1993) and has been tested against their version. The results of both codes are in excellent agreement on time scales relevant for the analysis herein.

The background magnetic field is considered to be homogeneous. The wave frequencies and wave numbers are obtained from the IDLWhamp code (Paesold 2002). The electric field strength E_i of one single wave i is treated as a free parameter, and the magnetic field components are calculated according to Faraday's law $\dot{\boldsymbol{B}}_i = -c\boldsymbol{\nabla}\times\boldsymbol{E}_i$. The simulations are split into two parts. First, the trajectories of single particles in a single wave have been computed. The results of these simulations are presented in Sect. 5.1. During a second set of simulations, groups of 500 particles have been followed in a spectrum of 500 waves. The results of this second set of simulations are presented in Sect. 5.2. The 500 monochromatic purely transverse waves are confined to a range of frequencies where the linear growth rate does not drop below ∼70% of the maximum growth rate. The applied wave spectrum corresponds to the spectrum depicted in Fig. 1 restricted to the range of ∼4.1−6.5 kc/ω_p.

It is assumed, that the electric field amplitude, normalized to the background magnetic field, of each wave is the same and its numerical value is treated as a free parameter. The wave fields are not present at the beginning of the simulation period. The fields are switched on adiabatically, linearly increasing over a time of $t = 1/\Omega_p$ until they reach the desired value. In the course of the analysis it turned out that, as soon as non-vanishing initial perpendicular velocities are taken into account, it is crucial for the final result to let the waves grow slow enough to ensure adiabaticity of the process. The plasma parameters throughout all simulations are $n_e = n_p = 5 \times 10^{10}$ cm^{-3}, $T_\perp^e = T_\perp^p = T_\parallel^p = 1 \times 10^7$ K, $T_\parallel^e/T_\perp^e = 13$ (see Fig. 1) and the background magnetic field is $B_0 = 100$ G. The anisotropy of the plasma is chosen such that the resulting wave field represents the situation close to instability threshold.

Since the wave frequencies are at about the gyrofrequency of the protons (see Fig. 1), the simulation time span has to cover at least a few tens of Ω_p^{-1} in order to sample several gyro periods of the waves. The time scale of interest for the electron motion lies at the inverse gyrofrequency of the electrons. The time steps of the simulation therefore have to be chosen to resolve the gyro period of the electrons. Since the real mass ratio $m_p/m_e \approx 1836$ is used, about 10^4 iterations per proton gyration have to be computed, resulting in a large computing effort.

A group of electrons, which initially can be described by a density peak in velocity space
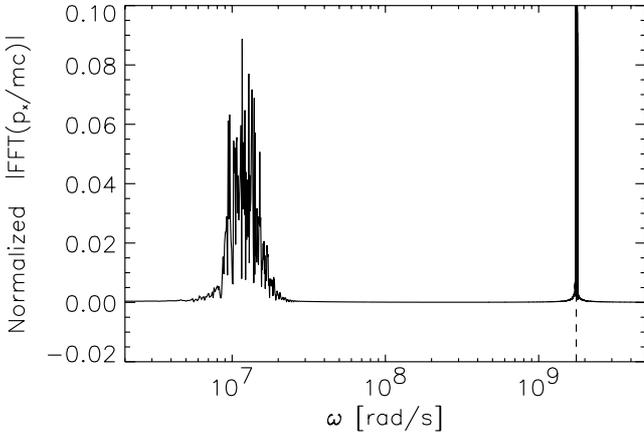
$$f(v_\parallel, v_\perp, t_0) \propto \delta(v_\parallel - v_\parallel^0) \times \delta(v_\perp - v_\perp^0), \quad (13)$$

is injected at $(v_\parallel^0, v_\perp^0)$ and is followed in time. Randomization of the electron gyro phases is achieved by choosing the initial

parallel coordinate to randomly vary along $\boldsymbol{B}_0$. It is assumed that all of the particles of one group experience the same wave field, i.e. the relative phases of the waves are not changed for one set of $(v_\parallel^0, v_\perp^0)$. For each set of initial velocities, an ensemble of 500 electrons is simulated during a time of $t \times \Omega_p = 40$.
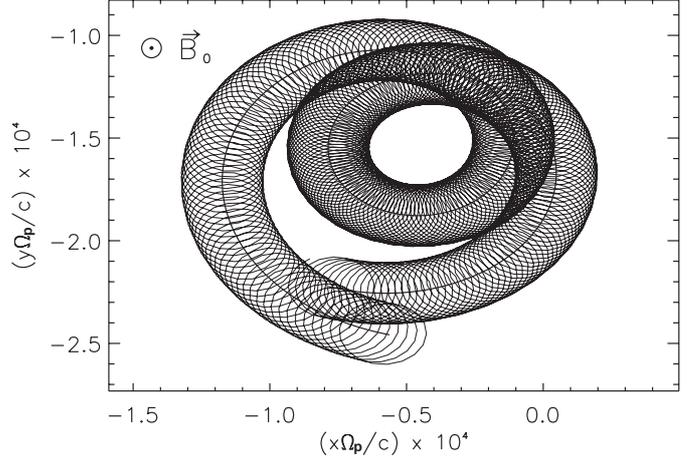
4.2. Simulation analysis

In order to analyze the motion of the gyro center in the test particle simulation, the gyro motion of the electrons has to be eliminated from the full particle motion. This is done by a Fast Fourier transformation, separating the different contributions in the time series of the components of space coordinates and momenta. The spectrum of a representative run is displayed in Fig. 2.
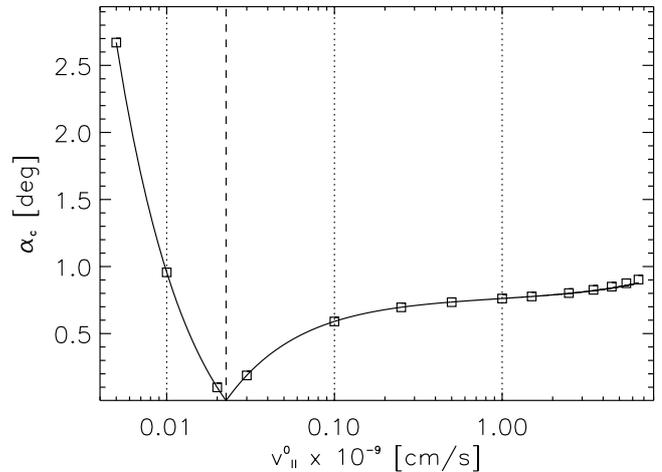

Fig. 3. Test particle trajectory in normalized coordinates. The thin line represents the full motion whereas the thick line is the reduced gyro center motion.

5. Results

5.1. Single wave simulation

Simulations in the field of a single wave are presented in order to establish the range of validity of the approximations derived in Sect. 3. Single electrons at several $v_\parallel^0$ are injected at random relative phases $\phi = \theta - \Psi$ into the field of a single wave with the properties $\omega/\Omega_p = 1$ and $kc/\omega_p = 4.33$, according to the linear dispersion of EF waves (see Fig. 1).

At vanishing initial perpendicular velocities $v_\perp^0$ the predictions of the theory and the results of the simulation are in excellent agreement (Fig. 4). The slight deviation towards large $v_\parallel^0$ is a result of loss of adiabaticity as the Doppler shifted frequency of the wave approaches the gyrofrequency of the electron in its parallel co-moving system. At particle speeds of $v_\parallel = \omega/k$ a minimum in pitch-angle is found. The minimum is exactly

Fig. 2. Power spectrum of x-component of the normalized momentum. The dashed line indicates the expected gyrofrequency of the electron. The group of peaks to the left represents the wave field, shifted to higher frequencies due to the parallel motion of the particle.

The peak at high frequencies is due to the gyro motion of the electron as indicated by coincidence with the electron gyrofrequency Ω_e. The peaks at lower frequencies represent the spectrum of the applied wave field. It is Doppler shifted to higher frequencies $kv_\parallel + \omega_k$ since the spectrum is taken in the parallel co-moving guiding center frame. At high enough parallel velocities, the spectrum of the wave field in Fig. 2 would be shifted to the gyration peak resulting in wave-particle resonance. This situation is excluded from this work by assuming initial parallel velocities small enough to ensure non-resonance.

A portion of an exemplary particle trajectory in the $x - y$ plane is displayed in Fig. 3. The gyration of the electron forces it into a fast spiral motion along the local magnetic field. In addition, its gyro center moves in a second, more irregular spiral. This second motion is much slower and superimposed on the unperturbed electron orbit. The gyro centers can be treated as unmagnetized quasi-particles. If not mentioned otherwise, we always refer to these quasi-particles when describing particle properties in the further analysis of the simulations.

Fig. 4. Pitch-angle increase of quasi-particles at several initial parallel velocities $v_\parallel^0$ by the interaction with a single wave. The initial perpendicular velocity $v_\perp^0$ equals zero. The solid line represents the results obtained from Eqs. (4) and (5) whereas the squares confer to the results of the simulation. The electric field strength of the wave is $\hat{e}/B_0 = 10^{-5}$.
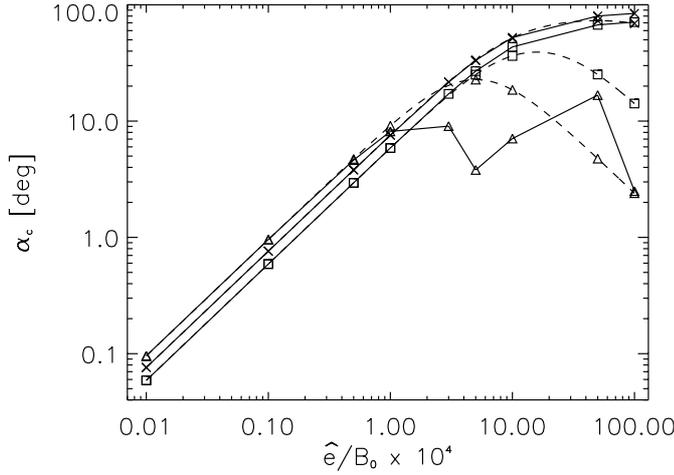
Fig. 5. Plot of pitch-angle increase vs. electric wave field. The symbols here refer to different initial parallel velocities indicated in Fig. 4 by vertical dotted lines: triangle $v_\parallel^0 = 10^7$ cm/s, square $v_\parallel^0 = 10^8$ cm/s and cross $v_\parallel^0 = 10^9$ cm/s. The dashed curve shows the results from Eq. (7). The symbols close to the dashed curves are the results of the simulations for $v_\perp^0 = 0$. Solid lines connect the results obtained from the simulations for $v_\perp^0 = 1.5 \cdot v_{\text{th}}$.

located at v_{crit} as predicted by Eq. (6). The critical velocity v_{crit} is indicated by a vertical dashed line in the plot.

The dependence of the pitch-angle increase α_c on the wave field strength $\hat{e}$ is shown in Fig. 5. The theoretical predictions are compared with results of the simulations at three different initial parallel velocities $v_\parallel^0$. Simulation results for vanishing initial perpendicular velocity fall all very close to the values predicted by the analytical drift approximation. The theoretically approximated and simulated values show excellent agreement over 4 orders of magnitude up to magnetic wave field strengths of order $10 \times B_0$. Although these values are unreasonably high when dealing with waves resulting from linearized kinetic theory, the results clearly show, that the drift approximation is valid on all scales of field strength as long as the initial gyro motion of the electron vanishes.

The situation is different if $v_\perp^0 \neq 0$ is assumed. Equation (7) would predict that the resulting α_c is independent of $v_\perp^0$. As can be seen in Fig. 5, this is only true for values of the electric wave field below $\hat{e}/B_0 \approx 10^{-4}$. Larger fields cause loss of adiabaticity and the approximation therefore becomes invalid. The situation differs depending on the value of $v_\parallel^0$: adiabaticity is lost first at small values (Fig. 5, triangles) when increasing $\hat{e}$. At larger $v_\parallel^0$ values the analytic description yields a good approximation even for large values of $\hat{e}$ (Fig. 5, crosses).

The upper boundary for the analytical approximation to be valid is at an electric wave field of $\hat{e}/B_0 \approx 10^{-4}$. This corresponds to a wave magnetic field of 1.3% of the background magnetic field in the case of EF waves. When increasing the field strength beyond this value, the resulting drifts and displacements in velocity space cannot be predicted anymore by Eqs. (4) and (5). According to Fig. 5 this corresponds to a maximum pitch-angle displacement of about 10 deg that can be described by the approximation.
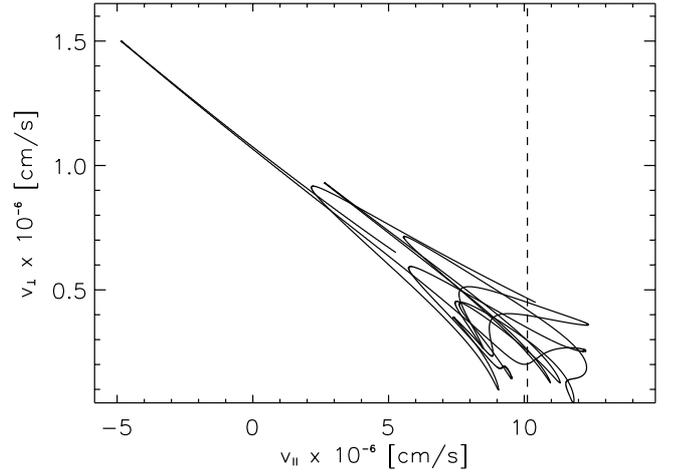

Fig. 6. Trajectory of a quasi-particle in a EF wave spectrum with a rms-field of $E_{\text{rms}}/B_0 \sim 2.2 \times 10^{-5}$. The vertical dashed line indicates the parallel initial velocity.

5.2. Wave spectrum simulation

When assuming a spectrum of EF waves, several aspects of the model change. Figure 6 is a part of the trajectory of a quasi-particle that started at $v_\perp^0 = 0$ and $v_\parallel^0$ as indicated by the dashed line. As can be seen in Fig. 6 the trajectory of the quasi-particles in velocity space becomes irregular and takes excursions to negative parallel velocities. The most important reason is the influence of the first adiabatic invariant, the conservation of the magnetic moment μ, described in Sect. 3, Eq. (10). Contrary to the case of the single wave simulation, the magnitude of the total magnetic field is a function of time and space and therefore redistributes the perpendicular and parallel velocities. Combined with the long-term conservation of energy, the invariance of μ causes a stochastic element in the simulation. The resulting displacement in velocity space depends on the time history of $|\boldsymbol{B}|$, i.e. the total change in $|\boldsymbol{B}|$ a particle experiences. This only depends on the initial conditions, i.e. the relative phases in the wave field and the relative phase of the electron, and is therefore random for each particle. Another aspect of $|\boldsymbol{B}|$ being a function of time is that the range of validity of the approximation is not as clearly defined as in the case of a single wave. Even though the rms-value of the total perpendicular electric wave field lies well in the valid range, the instantaneous electric field can take an excursion far above the limit. Particles experiencing such excursions do not behave adiabatically anymore and severely alter the statistics of the ensemble.

In the case of very weak wave field strengths, the drift approximation still yields a good prediction of the pitch-angle behavior of an ensemble of electrons in a spectrum of EF waves. The results of such simulations is shown in Fig. 7a. The electric field strength of a single wave is $\hat{e}_k/B_0 = 10^{-6}$, corresponding to a rms value of the total perpendicular electric field of $E_{\text{rms}}/B_0 \approx 2.2 \times 10^{-5}$. The symbols here and throughout the rest of this section refer to different perpendicular initial velocities as follows: diamond $v_\perp^0 = 0$, triangle $v_\perp^0 = 0.5 \cdot v_{\text{th}}$, cross $v_\perp^0 = v_{\text{th}}$ and asterisk $v_\perp^0 = 1.5 \cdot v_{\text{th}}$. Since the results of the simulation do not depend on $v_\perp^0$ at higher $v_\parallel^0$, only a few representative values
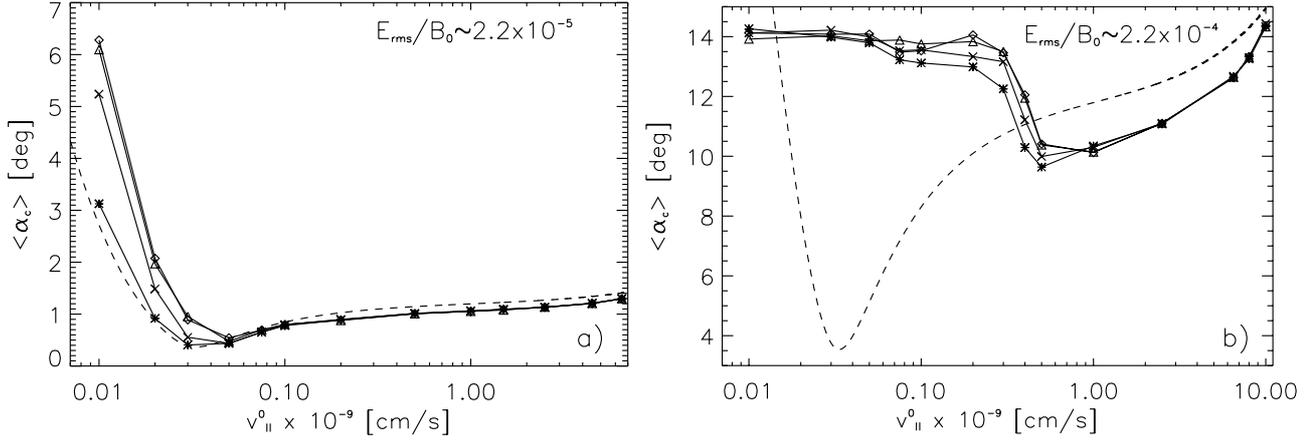
Fig. 7. Mean pitch-angle α_c due to interaction with a spectrum of EF waves. Sets of 500 electrons at several initial velocities $(v_\parallel^0, v_\perp^0)$ have been simulated. The initial values for the gyro centers are thus given by $(v_\parallel^0, 0)$. The dashed curve represents the analytic results obtained from Eqs. (7), (8) and (9) whereas the symbols confer to the results of the simulation for different $v_\perp^0$ (notation see text). *Left:* the rms electric field amplitude of the total perpendicular wave field is $E_{\rm rms}/B_0 \approx 2.2 \times 10^{-5}$. *Right:* $E_{\rm rms}/B_0 \approx 2.2 \times 10^{-4}$.

are plotted. At higher parallel velocities Eqs. (7), (8) and (9) well approximate the simulated data. The simulation deviates from the theoretically approximated values at smaller $v_\parallel^0$ and the resulting pitch-angles exhibit a dependence on the initial perpendicular speed.

The deviation becomes more and more significant when increasing the electric wave fields. A simulation with strong wave fields of $\hat{e}_k/B_0 = 10^{-5}$, corresponding to a total perpendicular electric field of $E_{\rm rms}/B_0 \approx 2.2 \times 10^{-4}$, is depicted in Fig. 7b. The simulation exhibits a behavior completely different from what is expected by the drift approximation. Only at the largest initial parallel velocities the simulation approaches the analytical approximation. The mean pitch-angle shift by interaction with the wave field does not significantly depend on the initial perpendicular speed $v_\perp^0$. The value of $v_\parallel^0$ below which the simulation breaks away from the qualitative behavior expected from the drift approximation linearly depends on the wave field strength. Additional simulations in the range up to $\hat{e}_k/B_0 = 10^{-5}$ not shown here have been carried out to confirm this dependence.

Having investigated the motion of the gyro centers, the situation of the real electrons has to be studied now. The full trajectories of the same simulations as above are analyzed and the resulting displacement of the real electrons in pitch-angle is shown in Fig. 8. The change in pitch-angle is shown for simulations with an rms-value of the total perpendicular electric field of $E_{\rm rms}/B_0 \approx 2.2 \times 10^{-4}$, corresponding to Fig. 7b. The dashed curves refer to the values of one standard deviation added to the mean. These values are positive throughout the whole plot, as the distribution is broad. Note: the pitch-angle distribution is not normally distributed.

6. Discussion

The discussion of the results presented in the preceding section is split into two parts. First, the single wave simulation results are discussed separately and in short, whereas the case of the wave spectrum needs to be addressed more extensively.
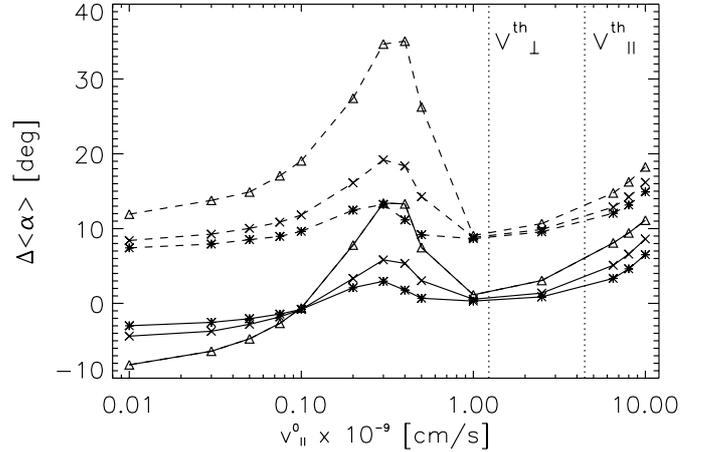
Fig. 8. Change in the mean pitch-angle α of the real electrons by interaction with a spectrum of EF waves vs. the initial parallel velocity $v_\parallel^0$. The symbols are the same as in Fig. 7. Solid lines represent the average values $\langle \Delta\alpha \rangle$, whereas the dashed lines indicate the distribution $\langle \Delta\alpha \rangle + \sigma$ for the simulations displayed in Fig 7b. For comparison, vertical dotted lines indicate the perpendicular and parallel thermal velocity of the electron distribution.

In the case of the single wave simulation, the findings are in good agreement in a limited range with the expectations derived from the analytic drift kinetic approach discussed in Sect. 3. Assuming vanishing perpendicular initial velocities, the predictions of the theory are in excellent agreement with the simulations on all scales of wave field strengths. The assumption of finite values of $v_\perp^0$ yields a limit in the range of validity of the drift approximation: At low wave fields no difference between finite and vanishing $v_\perp^0$ is observed. By increasing the wave amplitudes above a value of $e_k/B_0 \approx 10^{-4}$, the approximation breaks down (Fig. 5). The deviation becomes significant first at the lowest initial parallel speeds. The value $e_k/B_0 \approx 10^{-4}$ corresponds to a wave magnetic field of $\approx 13\%$ of the background magnetic field and is concluded to be the

limiting field strength for the assumption of adiabaticity in the investigated system.

The case of the wave spectrum simulation requires more extensive discussion than the above. Many effects are observed resulting in deviations from the predictions of the drift approximation. As can be seen in Fig. 7, the drift approximation deviates from the simulation first at small initial parallel velocities. When increasing the wave fields, the point where the approximation breaks away from the simulation is shifted to larger values of $v_\parallel^0$. These observations are discussed in detail in the following and possible causes of the deviations are presented.

The major aspect, that has changed in the transition from a single wave to a spectrum of waves, is the time dependence of $|B|$. While in the case of a single wave the total magnetic field of the wave is constant in time, the superposition of the single waves in the spectrum causes the total magnetic field to vary in space and time. Several new effects result from this. As mentioned in Sect. 3, the change in $|B|$ with time results in additional shifts in velocity space due to the conservation of the magnetic moment, i.e. Eq. (10). The particles are shifted to smaller parallel velocities when the value $|B|$ increases and, if the change is large enough, can therefore be displaced to even negative parallel speeds. This causes large excursions in pitch-angle and severely alters the statistics of the ensemble. The mean is shifted to larger values than expected from the approximation. The conservation of magnetic moment surely influences the simulation but is not included in the analytical approximation. Yet, it cannot account for all effects in the simulation. The significant dependence on $v_\perp^0$ that is predicted by Eq. (10) is not observed in the simulation (see Fig. 7b). There is no systematic dependence on the initial perpendicular speed in the simulation.

The above assumes that the change in $|B|$ is such that adiabaticity is conserved and, hence, the magnetic moment is conserved. Single wave simulations yield as a necessary condition for the validity of the drift kinetic approximation that $e_k/B_0 \lesssim 10^{-4}$. While the rms-value of the total electric field also lies around that value for the simulation presented in Fig. 7b, the momentary field can take rather large excursions and typically reach two to three times the rms-value. This causes loss of adiabaticity and therefore results in pitch-angle scattering that cannot be explained by the drift approximation. As can be seen from the single wave simulation in Fig. 5, adiabaticity is lost first at small initial parallel speeds while the approximation holds for large $v_\parallel^0$. The largest deviations from the theoretically approximated values occur at small initial parallel velocities. At larger speeds the approximation is still valid within a 15% range. Due to the faster motion the particle feels the excursions less than the slow particles.

To illustrate the stochastic behavior in the simulation, an exemplary Poincaré map for a small ensemble of 70 quasi-particles is presented in Fig. 9. The procedure follows Karimabadi et al. (1989). The transition to canonical coordinates yields $P_\parallel = p_\parallel$ and $P_\perp = p_\perp + q/c \cdot A$ for parallel and perpendicular momentum, respectively; p_i refers to the physical momentum and A is the vector potential defined as $(c/\omega)(\hat{e} \sin\Psi, -\hat{e}\cos\Psi + xB_0, 0)$ according to the definition of δB and B_0 in Sect. 3. A surface in the phase space is defined
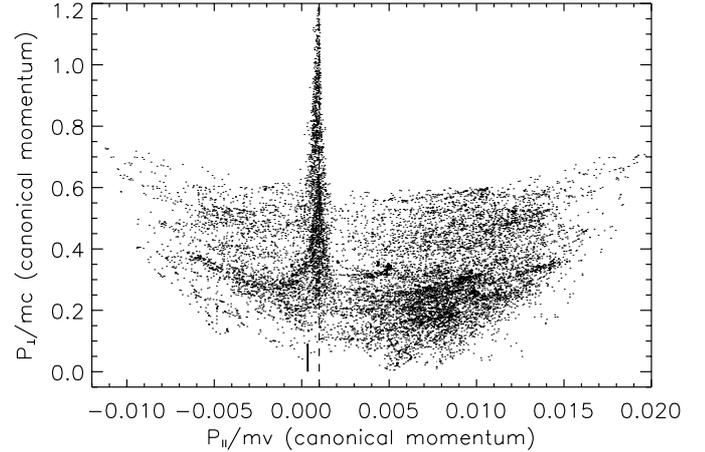
Fig. 9. Poincaré map of an ensemble of 70 quasi-particles with initial momenta indicated by the vertical bar near (0,0). The initial parallel speed is $v_\parallel^0 = 1 \times 10^7$ cm/s. The surface in phase space is defined by equating the phase of the particles to zero, i.e. $\theta = 0$. The vertical dashed line indicates the position of the minimum in the gyro center pitch-angle α_c at v_{crit} obtained from Eqs. (7), (8) and (9).

by equating the phase angle θ of the gyro centers to zero. The dots in the plot therefore represent the phase angle $\theta = 0$ for all particles throughout the temporal history of the simulation. The thick black bar indicates the initial values of the real electrons. The finite width in perpendicular direction is a result of the xB_0 term in the y-component of the vector potential A.

The particles fill an area in phase space that is much larger than expected from the drift motion derived in Sect. 3. In particular it can be seen that a significant fraction of particles is scattered to negative parallel velocities. A new feature becomes apparent which has not been addressed yet: the particles concentrate and become over-dense in the region around v_{crit} (Fig. 9). Instead of systematically interacting with the wave and experiencing the helical motion in the wave's magnetic field, the particles feel a randomly fluctuating field at v_{crit}. This results in anomalous stochastic increase in perpendicular velocity. By investigating Poincaré maps at several parallel initial velocities, it turns out that the point where the approximation breaks away from the simulation is determined by the size of the attractive area of the minimum. A full treatment of the stochasticity of the system lies beyond the scope of this paper and is a topic for future work. Nevertheless, from the work presented here it follows that stochastic effects occur at the pitch-angle minimum predicted by the drift approximation, causing anomalous pitch-angle displacements.

The quantities of interest for the resulting pitch-angle development and isotropization of the electron distribution are the pitch-angles of the real electrons. The change in pitch-angle is generally larger for smaller initial perpendicular velocities. This tendency is observed throughout the simulation. It reaches a maximum in the special case of vanishing $v_\perp^0$ which is not shown in Fig. 8. Electrons starting at $v_\perp^0 = 0$ experience the strongest increase in pitch-angle and behave differently from the other particles. However, zero perpendicular speed is a very

special state for an electron and not relevant to the bulk reaction of the whole electron population.

The displacements in the mean of pitch-angles are depicted in Fig. 8. Three different regions can be identified: below a value of about $v_\parallel^0 \approx 10^8$ cm/s, the mean pitch-angle is shifted to lower values, in the intermediate range from $v_\parallel^0 \approx 10^8 - 10^9$ cm/s there is a local maximum and above a value of $v_\parallel^0 \times 10^{-9} \approx 10^9$ cm/s the pitch-angle displacement continuously increases with increasing $v_\parallel^0$. The latter one is interpreted as the increase by approaching resonances with the wave field starting at around $\sim 2 \times 10^{10}$ cm/s. Nevertheless, the interaction is non-resonant and belongs to the isotropization process to be investigated by this work. The result is a fan-like widening of the faster electrons with parallel velocities beyond the perpendicular thermal speed. At even higher initial velocity, this behavior dominates the isotropization process, ultimately yielding resonant pitch-angle scattering as observed in Messmer (2002).

The most interesting region from the point of view of non-resonant interaction is the region below $v_\parallel^0 \approx 10^9$ cm/s. No resonances are present in this range and the response of the electrons is not expected to exhibit a strong dependence on the single particle kinetics. Nevertheless, Fig. 8 indicates a significant dependence on the initial parallel speed. Two regimes can be distinguished here: a negative shift below around $v_\parallel^0 \approx 10^8$ cm/s and a positive shift above it. The negative shift at low $v_\parallel^0$ is of comparable magnitude to the positive shift in the intermediate range. Shifts at low parallel velocity have little effect on the anisotropy and mainly smooth the distribution at $\sim 90°$ pitch-angle. In the intermediate range, stronger displacement in pitch-angle is observed and due to smaller, while still large, initial pitch-angles α_0 more energy is transferred to the perpendicular direction.

The time scales for the displacement in pitch-angle are related to the growth of the EF waves. Since the process is assumed to be adiabatic, at least in the ranges described in the above, the particle changes directly follow the growing waves. Hence, the characteristic time scale for the pitch-angle shift is given by the inverse of the linear growth-rate $\tau \sim 1/\gamma$ which is of order $\sim 1/\Omega_p$ in the case of EF waves.

The simulations assume infinite coherent wave fields. In reality an electron will move into a region of space with entirely different wave phases within a time $\tau_c \approx \Delta z(\omega)/v_\parallel^0$, where $\Delta z(\omega)$ is the spatial dimension of coherent wave packets with frequency ω. The size is determined by the formation of these waves, the EFI. The instability operates coherently on dimensions of $\Delta z(\omega) \ll f/\nabla_x f$, where f is the electron distribution. For a scale length of 10^5 cm in the acceleration region, Δz may be roughly estimated to be 10^4 cm and thus $\tau_c \approx 10^{-5}$ or a few proton gyro periods. This is consistent with the assumptions of the simulation of constant wave phases.

On the other hand, the above rough estimate suggests that an electron rapidly moves through regions with different wave phases. Every time it does so, scattering starts anew. The simulations show that in each step the pitch-angle increases a few degrees in the favorable regions of velocity space.

7. Conclusions

It has been established in a former work (Paesold & Benz 1999) that the Electron Firehose instability (EFI) can arise as a result of electron acceleration in impulsive solar flares. For a velocity space anisotropy ($T_\perp < T_\parallel$) in the accelerated electron distribution, Electron Firehose (EF) waves are non-resonantly excited.

The kinetic response of the electrons to the non-resonant instability in terms of pitch-angle development is investigated in the work presented herein. Test particle simulations are carried out that are interpreted by a drift kinetic approach. The results clearly show that electrons are non-resonantly scattered to higher pitch-angles. It is caused by $E \times B$ drift, curvature drift and approximate conservation of magnetic moment.

At small wave field strengths the drift kinetic approach yields a good approximation to the system in both an electron in a single wave and in a spectrum of waves. By increasing the field strength in the single wave simulation, an upper limit for the validity of the drift approximation is found at a value of $e_k/B_0 \approx 10^{-4}$. As a result, computing efforts can be greatly reduced for $e_k/B_0 < 10^{-4}$ in future analyses by directly simulating the slow-scale motion in the drift kinetic equations. This is not the case for a spectrum of waves since the limit is not clearly defined. Due to variations in the magnitude of the total magnetic field $|B|$ adiabaticity can only be ensured for very small field strengths. At larger values of e_k the electron orbits become stochastic and the resulting pitch-angle displacement cannot be described by the approximation.

In support of this conclusion, it is found that the particle response to the EF waves exhibits variations dependent on the particle velocities. Although the instability is hydrodynamic and does therefore not depend on single electron kinetics, a pronounced dependence of the electron response on the initial parallel velocity is observed. It is expected that some intermediate velocities and very fast velocities isotropize more rapidly. Thus the evolution of the particle distribution in velocity space can develop peculiar shapes rather than maintaining an ellipsoidal form.

The simulations show that the isotropization needed in a solar particle acceleration context cannot be achieved in one step by a single set of waves. Nevertheless, the spatial inhomogeneity in the acceleration region causes a frequent change in the wave's phase relations resulting in multiple scattering capable of isotropizing the electron distribution at a rate that is required for electron acceleration in solar flares.

References

Birdsall, C. K., & Langdon, A. B. 1991, Plasma Physics via Computer Simulation (Institute of Physics Publishing, Bristol and Philadelphia)
Brown, J. C. 1971, Sol. Phys., 18, 489
Fisk, L. A. 1976, J. Geophys. Res., 81, 4633

Hasegawa, A. 1975, Plasma Instabilites and Nonlinear Effects Berlin (Heidelberg New York: Springer Verlag)

Hollweg, J. V., & Völk, H. J. 1970, J. Geophys. Res., 75/28, 5297

Karimabadi, H., Akimoto, K., Omidi, N., & Menyuk, C. R. 1989, Phys. Fluids B, 2(3), 606

Kiplinger, A. L., Dennis, B. R., Frost, K. J., & Orwig, L. E. 1984, ApJ, 287, L105

Lenters, G. T., & Miller, J. A. 1998, ApJ, 493, 451

Leroy, M. M., & Mangeney, A. 1984, Ann. Geophys., 2, 4, 449

Li, X., & Habbal, S. R. 2000, J. Geophys. Res., 105/A12, 27377

Messmer, P. 2002, A&A, 382, 301

Miller, J. A. 1997, ApJ, 491, 939

Miller, J. A., & Viñas, A. F. 1993, ApJ, 412, 386

Miller, J. A., LaRosa, T. N., & Moore, R. L. 1996, ApJ, 461, 445

Miller, J. A., Cargill, P. J., Emslie, A. G., et al. 1997, J. Geophys. Res., 102/A7, 14631

Moore, R. L., & Fung, P. C. W. 1972, Sol. Phys., 23, 78

Paesold, G. 2002, E-Collection ETH, http://e-collection.ethbib.ethz.ch/

Paesold, G., & Benz, A. O. 1999, A&A, 351, 741

Parker, E. N. 1958, Phys. Rev., 109, 1874

Pilipp, W., & Völk, H. J. 1971, J. Plasma Phys., 6, 1

Rönnmark, K. 1982, KGI Rep., 179

Stix, T. H. 1992, Waves in Plasmas, New York AIP, 273

Sturrock, P. A. 1980, Solar Flares: A Monograph from Skylab Solar Workshop II (Boulder: Colorado Assoc. Univ. Press)

Vaiana, G. S., & Rosner, R. 1978, ARA&A, 16, 393

Wu, C. S. 1984, J. Geophys. Res., 89/A10, 8857